## Analysis of localized surface plasmon resonance in glass-supported gold nanoparticles with a hexagonal pattern

Hajebifard, Akram; Yuan, Jie; Zou, Shan; Berini, Pierre



**Publisher's version / Version de l'éditeur:**
https://doi.org/10.1117/12.2042346
*Photonics North 2013, 2013-10-11*

# Analysis of localized surface plasmon resonance in glass-supported gold nanoparticles with a hexagonal pattern

Akram Hajebifard, Jie Yuan, Shan Zou, Pierre Berini

Akram Hajebifard, Jie Yuan, Shan Zou, Pierre Berini, "Analysis of localized surface plasmon resonance in glass-supported gold nanoparticles with a hexagonal pattern," Proc. SPIE 8915, Photonics North 2013, 89151M (11 October 2013); doi: 10.1117/12.2042346

SPIE.

Event: Photonics North 2013, 2013, Ottawa, Canada

# Analysis of Localized Surface Plasmon Resonance in Glass-supported Gold Nanoparticles with a Hexagonal Pattern

Akram Hajebifard[a*], Jie Yuan[b,c], Shan Zou[c], Pierre Berini[a,d]

[a] Department of Physics, University of Ottawa, 150 Louis Pasteur, Ottawa, Canada, [b]Department of Chemical and Biological Engineering, University of Ottawa, 161 Louis Pasteur, Ottawa, Canada, [c] National Research Council Canada, 100 Sussex Dr., Ottawa, Canada, [d] School of Electrical Engineering and Computer Science, University of Ottawa, 800 King Edward Ave, Ottawa, Canada,

## ABSTRACT

An approach has been devised to create a hexagonal pattern of glass-supported gold nanoparticles (AuNPs) with controllable particle size and inter-particle spacing, by combining the self-assembly of block copolymer micelle-loaded metal precursors with a seeding growth method. Absorbance spectra as an optical response of the AuNP arrays were measured to obtain their LSPR peak position ($\lambda_{LSPR}$). There was a red shift in $\lambda_{LSPR}$ with increasing cover medium refractive index for all fabricated and simulated arrays. A comparison between computed and measured $\lambda_{LSPR}$ for a 33 nm AuNP array suggests that large nanoparticles produced by this fabrication method have ellipsoidal shapes rather than spherical ones, as in the case of small AuNP arrays.

**Keywords:** gold nanoparticles (AuNPs), localized surface Plasmon resonance (LSPR), self-assembly, diblock copolymer, seeding growth, embedding ratio, COMSOL, absorbance spectra

## INTRODUCTION

The surface plasmon resonance of gold nanoparticles (AuNPs) in the visible range of the electromagnetic spectrum has made them excellent candidate structures for use in various applications such as, solar energy harvesting, lasing and sensing applications.[1-5] However, the fabrication of ordered arrays of metal nanoparticles over a large area with controllable particle size and spacing is challenging. Some researchers have focused on producing metal nanoparticle arrays over large areas using several methods[6-9], but many difficulties remain, including control over particle size and spacing. Using diblock copolymer micelles loaded by metal precursors, Möller *et al.* introduced the method of forming NP arrays on solid supports.[10] This approach is not only simple and cost-friendly, but also can produce a continuous array "sheet" of NPs of uniform size over a large area.[11-13] The fabrication approach used herein for producing AuNPs is based on this method combined with a seeding growth technique.[14] In this paper we give additional computation details and results describing the optical performance of such NPs.

The metal NP's optical response is determined to a great extent by the localized surface plasmon resonances (LSPRs) supported thereon. The peak of such resonances has been widely used in sensing applications by monitoring its location over time by measuring absorbance, scattering or extinction spectra.[15, 16] Sensitive to the optical properties of the surrounding environment, LSPRs are charge density oscillations on metal NPs excited by light - metal NPs can scatter and absorb electromagnetic waves. According to the Mie theory,[17] for small metal NPs, the extinction, absorption and scattering cross-sections are given by:[18]

$$c_{abs} = k\,\mathrm{Im}(\alpha) \tag{1}$$

$$c_{scat} = \frac{1}{6\pi} k^4 |\alpha|^2 \tag{2}$$

* ahaje092@uottawa.ca; phone 1 613 400-6590;

Photonics North 2013, Pavel Cheben, Jens Schmid, Caroline Boudoux, Lawrence R. Chen, André Delâge, Siegfried Janz, Raman Kashyap, David J. Lockwood, Hans-Peter Loock, Zetian Mi, Eds., Proc. of SPIE Vol. 8915, 89151M · © 2013 SPIE · CCC code: 0277-786X/13/$18 · doi: 10.1117/12.2042346

$$c_{ext} = c_{abs} + c_{scat} \quad (3)$$

$$\alpha = 4\pi R^3 \left(\frac{\varepsilon_m - \varepsilon_d}{\varepsilon_m + 2\varepsilon_d}\right) \quad (4)$$

$$k = \frac{2\pi}{\lambda_0}\sqrt{\varepsilon_d} \quad (5)$$

where $\lambda_0$ and R are the free-space wavelength and the NP radius, respectively. $\varepsilon_d$ is the dielectric constant of the surrounding medium, and $\varepsilon_m = \varepsilon_1 + i\varepsilon_2$ is metal's dielectric constant ($e^{-j\omega t}$ time-harmonic form implied). For a good plasmonic metal ($\varepsilon_2 << \varepsilon_1$) the extinction, absorption and scattering are maximum at the wavelength where $\varepsilon_1 = -2\varepsilon_d$. For the case of the dipolar LSPR; we denote this wavelength as $\lambda_{LSPR}$. For small NPs with a diameter of 12, 25 and 34 nm (as studied in this work), absorption dominates,[19, 20] as shown in Figure 1. Therefore, absorbance spectra have been measured and computed for these nanoparticles to describe their optical response.

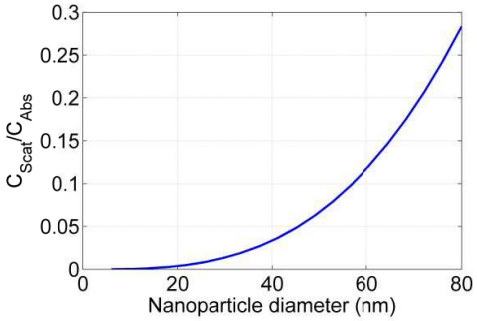


Figure 1 $C_{Scat}/C_{Abs}$ (scattering cross-section to absorption cross-section) as a function of NP diameter

## FABRICATION AND MEASUREMENTS

We have developed a fabrication method to produce hexagonal patterned AuNP arrays on glass – combined self-assembly and seeding-growth.[14] As displayed in Figure 2, gold salt loaded poly(styrene(48.5k)-*b*-2-vinyl pyridine(70k)) (PS-*b*-P2VP), Polymer Source Inc., Montreal, QC, Canada) micelles are spin-coated on glass coverslip substrates, and self-assembled in hexagonal patterned arrays. After the polymer shell is removed by oxygen plasma etching, AuNP "seed" arrays with NP sizes of 3, 5 or 10 nm are obtained. Chemically growing the "seed" arrays generates large AuNPs, up to 34 nm, while preserving the hexagonal pattern and centre-to-centre spacing.

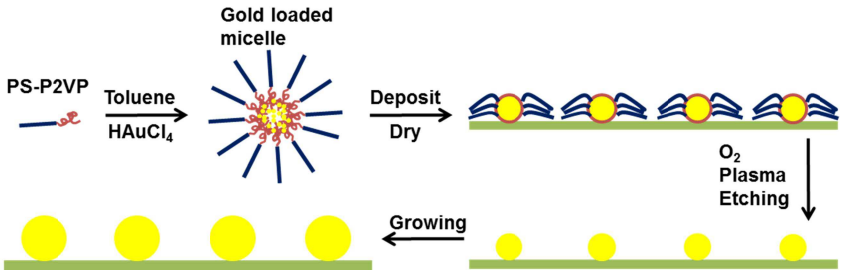


Figure 2 Fabrication procedure of hybrid diblock copolymer self-assembly and seeding-growth method.

Various solvents have been used in our measurements to provide cover media with different refractive indices. The solvents used in this paper are *o*-Dichlorobenzene (A), Toluene (F), Chloroform (G), Dichloromethane (H), Heptane (I), Ethanol (J), Water (K), Methanol (L), and Air (M), with refractive indices of 1.5514, 1.4969, 1.4458, 1.4241, 1.3876,

1.3614, 1.333, 1.3284, and 1.000, respectively. Also different mixtures of toluene and o-dichlorobenzene were prepared to provide media of refractive index 1.5460, 1.5351, 1.5242, and 1.5133 (identified as solvents B, C, D and E, respectively).

A fabricated AuNP array with mean height of 25.2 ± 4.0 nm and the edge-to-edge inter-particle spacing of 37 nm is presented in Figure 3(A). A 10 nm AuNP array with center-to-center inter-particle spacing of 62 nm was used as the "seed" array to further grow the AuNPs by controlling the concentration and growth time.[14] For 15 minutes of growth, a ~25 nm AuNP array was obtained. Figure 3(B) shows the absorbance spectrum of this array for different cover media, which illustrates a red shift in $\lambda_{LSPR}$ with increasing cover medium refractive index.

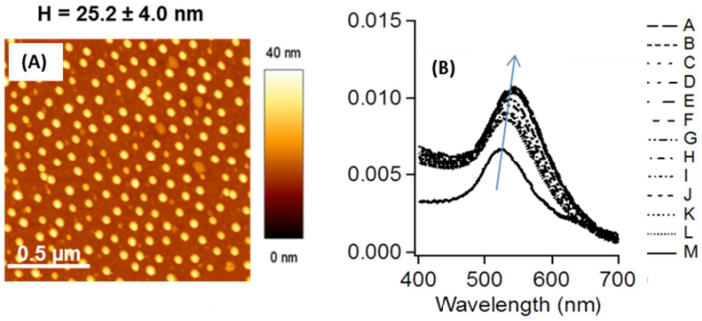


Figure 3 (A) AFM height image and (B) absorbance spectra of ~25 nm AuNP arrays. The blue arrow line indicates $\lambda_{LSPR}$ red-shifting.

## COMPUTATIONS

Computations have been carried out for AuNPs of 10, 25.7 and 33 nm, and the results compared with the experimental data.[14] In this paper, we present additional computations to illustrate that large nanoparticles, *e.g.,* 33 nm, fabricated by the method described above (and in greater detail in Ref. 21), behave like ellipsoids rather than spheres. To do so, $\lambda_{LSPR}$ of a fabricated 33 nm AuNP array was measured for different cover medium, and then compared with the computed results assuming arrays of spherical and oblate spheroidal AuNPs. The former includes AuNPs 33 nm in diameter, while the latter involves AuNPs with an ellipsoidal shape having a ratio of major to minor axes of 1.06. So, for the ellipsoid, the longitudinal diameter along the glass-cover medium interface is 35 nm and the transverse one is 33 nm. The edge-to-edge inter-particle spacing was 27 and 25 nm for the spherical and ellipsoidal AuNPs, respectively.

In our computations, it is assumed that the AuNP array includes an infinite number of particles of the same shape and inter-particle distance. The averaged geometrical properties of a sample was determined by AFM, and then used in the computations. As sketched in Figure 4(A), gold nanoparticles on glass are arranged in a quasi-hexagonal pattern, which results in a repeated parallelogram unit cell.

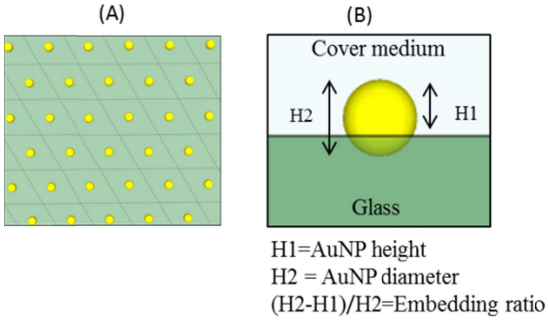


Figure 4 (A) A AuNP array fabricated on glass has a quasi-hexagonal pattern made of a repeated parallelogram-shape unit cell. (B) A AuNP embedded into glass.

To decrease the computational processing time, symmetry is exploited and one unit cell only involving one NP is simulated. Scattering boundary conditions have been applied on the top and bottom of the unit cell's boundaries. This kind of boundary prevents reflections into the domain and allows an incident plane wave to be defined. For the lateral boundaries, periodic boundary conditions were applied. As measurements show, the fabricated AuNPs are embedded into the glass, probably due to the plasma treatment process. This phenomenon is modelled by embedding the NP into the glass, as demonstrated in Figure 4(B). An embedding ratio of 20% was assumed in our computations. This assumption is based on comparisons between experimental and computed bulk refractive index sensitivities for AuNP arrays.[14]

**Mesh**

To assess convergence of the analysis, different mesh sizes have been tested. A good discretization was determined in the metal and in the rest of the domain as a minimum mesh size of 0.8 and 3 nm, respectively. Over the spectral range of interest (400-700nm), the skin depth of gold is of the order of the particle size, motivating a mesh density within the gold domain as small as 0.8 nm.

**Optical properties of the materials**

Frequency-dependent complex refractive indices were used in the computations to model the optical performance of the materials. They have been measured over the wavelengths of interest for glass,[21] gold,[22] and some of our solvents,[23-25] such as methanol, water, ethanol, heptane, chloroform and toluene. To determine the refractive indices of materials at the wavelengths where data are not available, cubic spline interpolation functions were applied. For other solvents a wavelength-independent refractive index at $\lambda$ = 589 nm was used, thus 1.4241, 1.5514, 1.5133, 1.5242, 1.5351, and 1.5460 were used as the refractive index for dichloromethane o-dichlorobenzene mixtures, T/D 3:7, T/D 1:1, T/D 7:3, T/D 1:9 respectively (T/D denotes the toluene/o-dichlorobenzene binary mixture).

As Boreman *et al.*[26] have shown, a combination of data from Palik[27] and Johnston and Christy[22] (JC) can be used as a best set of data for the optical properties of gold when modelling nanostructures. In this set, the imaginary part of the gold dielectric constant comes from JC, and the real part from JC and Palik. The real part of the dielectric constant over the spectral range of 400-500 nm was taken from Palik, while JC's data was used for the spectral range above 500 nm. Furthermore, gold's optical properties, which are size dependent, were modified for the nanoparticle sizes of interest, as shown in Figure 5.[28, 29] Utilizing these modified optical properties in the computations led to a good agreement between numerical and experimental results.[21]

As illustrated in Figure 5, the optical properties of AuNPs depend on their radius when the radius is small; radii of 3, 5, 11 and 15 nm are plotted in Figures 5A and 5B, along with the optical properties of bulk gold for comparison. Figure 5(A) and (B) illustrate that $-Re\{\varepsilon_{Au}\}$ and $-Im\{\varepsilon_{Au}\}$ are proportional and inversely proportional to the AuNP radius, respectively. To emphasise this point clearly, $-Re\{\varepsilon_{Au}\}$ versus AuNP's radius is plotted at $\lambda = 600\ nm$ in Figure 5(C), and Figure 5(D) shows $-Im\{\varepsilon_{Au}\}$ as a function of AuNP's radius at the same wavelength. Also, as seen in Figure 5(A), the negative real part of the gold dielectric constant ($-Re\{\varepsilon_{Au}\}$) increases with wavelength over the spectrum of interest. However, the negative imaginary part ($-Im\{\varepsilon_{Au}\}$) decreases with wavelength, as shown in Figure 5(B).

It is worth noting, from both Figure 5(C) and (D), that the slope of the plots is steeper for smaller radii than larger ones. This illustrates that the optical properties of smaller gold particles are more sensitive to the particle size than larger ones.

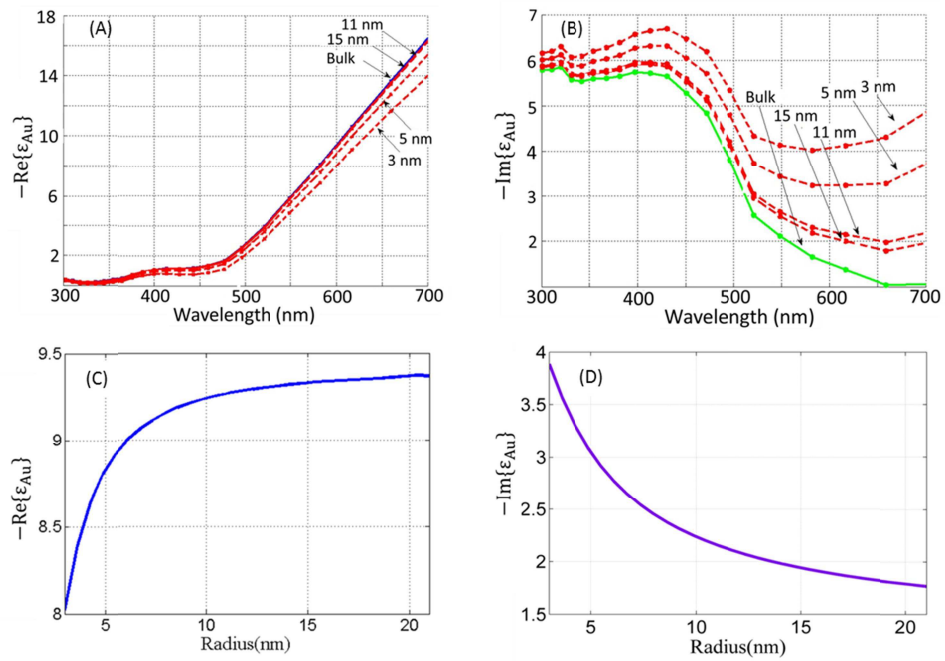


Figure 5 Size-dependent (A) real and (B) imaginary part of the gold dielectric constant; (C) $-\mathrm{Re}\{\varepsilon_{\mathrm{Au}}\}$ and (D) $-\mathrm{Im}\{\varepsilon_{\mathrm{Au}}\}$ versus AuNP radius at $\lambda = 600nm$ .

**Calculated absorbance on 33 nm AuNP array.**

The simulated structure was excited by a plane wave from the top, and the transmittance computed via a surface integral of the time-averaged pointing vector. Then the following equation was applied to calculate the absorbance $\mathrm{A} = -\log(\frac{\mathrm{T}}{\mathrm{T_0}})$ , where T is the transmittance with a nanoparticle in the unit cell, and $T_0$ is the transmittance without the nanoparticle in the unit cell.

In order to show the large fabricated nanoparticles (*e.g.*, 33 nm) have an ellipsoidal shape, a comparison between the measured and computed $\lambda_{\mathrm{LSPR}}$ was carried out. The absorbance spectra for 33 nm AuNPs of spherical and ellipsoidal shape are plotted in Figure 6(A) and (B). For both cases, the cover medium refractive index was changed from 1 to 1.5514 by assuming different solvents ranging from Methanol to o-Dichlorobenzene. The cover medium identified as M corresponds to Air. Strongly dependent on AuNP surrounding media, $\lambda_{\mathrm{LSPR}}$ shows a red shift with increasing cover medium refractive index for both AuNP arrays, as expected.[16, 28, 30-33]

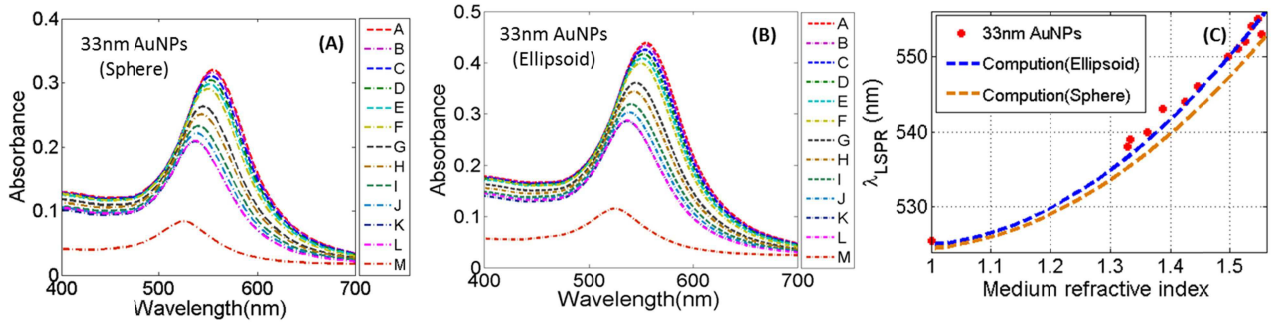


Figure 6 (A)-(B): Computational absorbance spectra of 33 nm AuNPs of (A) spherical and (B) ellipsoidal shape; (C) measured $\lambda_{\mathrm{LSPR}}$ versus cover medium refractive index for a fabricated 33 nm AuNP array and corresponding computed values for ellipsoidal and spherical AuNP arrays.

The computed $\lambda_{LSPR}$ versus cover medium refractive index is plotted for 33 nm spherical and ellipsoidal AuNP arrays in Figure 6(C). Also, this figure includes measured $\lambda_{LSPR}$ values versus cover medium refractive index for a fabricated 33 nm AuNP array. As noted from these results, the experimental data agrees better with the computations for the case of the ellipsoidal array. Therefore, the comparison indicates that fabricated AuNPs of 33 nm are more likely ellipsoidal than spherical, but only slightly as the aspect ratio of the ellipsoids was set to 1.06 in the computations.

## CONCLUSION

In conclusion, a method to fabricate hexagonal arrays of gold nanoparticles was discussed, in which diblock copolymer self-assembly followed by seeding growth was used to produce ordered AuNP arrays on glass substrates. The main advantage of this method is having control over the particle size and inter-particle spacing by tuning the metal precursors' loading ratio. We have shown that fabricated AuNPs with a diameter of about 33 nm have an ellipsoidal shape, by comparing the experimental $\lambda_{LSPR}$ with the computed ones over a large range of cover refractive indices. Conclusively, using post-seeding growth to enlarge AuNPs yields nanoparticles that are ellipsoidal rather than spherical in shape - however, the aspect ratio of the ellipsoids was only 1.06.

## REFERENCES


[1] Davis, T. J., Vernon, K. C. and Gomez, D. E., "Designing plasmonic systems using optical coupling between nanoparticles" Physical Review B 79(15), 155423 (2009).
[2] Vernon, K. C., Funston, A. M., Novo, C., Gomez, D. E., Mulvaney, P. and Davis, T. J., "Influence of Particle-Substrate Interaction on Localized Plasmon Resonances" Nano Letters 10(6), 2080-2086 (2010).
[3] Lopatynskyi, A., Lopatynska, O., Chegel, V., "Comparative analysis of response modes for gold nanoparticle biosensor based on localized surface plasmon resonance" Semiconductor Physics, Quantum Electronics & Optoelectronics 14(1), 114 (2011).
[4] Li, X., Yang, H., Xu, L., Fu, X., Guo, H. and Zhang, X., "Janus Micelle Formation Induced by Protonation/Deprotonation of Poly(2-vinylpyridine)-block-Poly(ethylene oxide) Diblock Copolymers" Macromolecular Chemistry and Physics 211(3), 297-302 (2010).
[5] Kim, H. M., Jin, S. M., Lee, S. K., Kim, M. and Shin, Y., "Detection of Biomolecular Binding Through Enhancement of Localized Surface Plasmon Resonance (LSPR) by Gold Nanoparticles" Sensors 9(4), 2334-2344 (2009).
[6] He, J., Kanjanaboos, P., Frazer, N. L., Weis, A., Lin, X. and Jaeger, H. M., "Fabrication and Mechanical Properties of Large-Scale Freestanding Nanoparticle Membranes" Small 6(13), 1449-1456 (2010).
[7] Martin, J. E., Wilcoxon, J. P., Odinek, J. and Provencio, P., "Control of the interparticle spacing in gold nanoparticle superlattices" J Phys Chem B 104(40), 9475-9486 (2000).
[8] Alivisatos, A. P., Johnsson, K. P., Peng, X. G., Wilson, T. E., Loweth, C. J., Bruchez, M. P. and Schultz, P. G., "Organization of 'nanocrystal molecules' using DNA" Nature 382(6592), 609-611 (1996).
[9] Park, S. Y., Lytton-Jean, A. K. R., Lee, B., Weigand, S., Schatz, G. C. and Mirkin, C. A., "DNA-programmable nanoparticle crystallization" Nature 451(7178), 553-556 (2008).
[10] Spatz, J. P., Roescher, A. and Moller, M., "Gold nanoparticles in micellar poly(styrene)-b-poly(ethylene oxide) films-size and interparticle distance control in monoparticulate films" Adv Mater 8(4), 337-340 (1996).
[11] Zou, S., Hong, R., Emrick, T. and Walker, G. C., "Ordered CdSe nanoparticles within self-assembled block copolymer domains on surfaces" Langmuir 23(4), 1612-1614 (2007).
[12] Lohmueller, T., Aydin, D., Schwieder, M., Morhard, C., Louban, I., Pacholski, C. and Spatz, J. P., "Nanopatterning by block copolymer micelle nanolithography and bioinspired applications" Biointerphases 6(1), MR1-MR12 (2011).
[13] Glass, R., Arnold, M., Cavalcanti-Adam, E. A., Blummel, J., Haferkemper, C., Dodd, C. and Spatz, J. P., "Block copolymer micelle nanolithography on non-conductive substrates" New Journal of Physics 6, 101 (2004).
[14] Yuan, J., Hajebifard, A., Berini, P., Zou, S., "Ordered gold nanoparticle arrays on glass and their characterization" Journal of Colloid and Interface Science (In press).

[15] McConnell, W. P., Novak, J. P., Brousseau, L. C., Fuierer, R. R., Tenent, R. C. and Feldheim, D. L., "Electronic and optical properties of chemically modified metal nanoparticles and molecularly bridged nanoparticle arrays" J Phys Chem B 104(38), 8925-8930 (2000).
[16] Kreibig, U., Volmer, M., [Optical Properties of Metal Clusters], springer-Verlag, Berlin (1995).
[17] Mie, G., "Articles on the optical characteristics of turbid tubes, especially colloidal metal solutions." Annalen Der Physik 25(3), 377-445 (1908).
[18] Liz-Marzán, L. M., "Nanometals: Formation and color" Materials Today 7(2), 26 (2004).
[19] Boyer, D., Tamarat, P., Maali, A., Lounis, B. and Orrit, M., "Photothermal imaging of nanometer-sized metal particles among scatterers" Science 297(5584), 1160-1163 (2002).
[20] Jain, P. K., Lee, K. S., El-Sayed, I. H. and El-Sayed, M. A., "Calculated absorption and scattering properties of gold nanoparticles of different size, shape, and composition: Applications in biological imaging and biomedicine" J Phys Chem B 110(14), 7238-7248 (2006).
[21]http://www.us.schott.com/advanced_optics/english/products/optical-materials/thin-glass/cover-glass-d-263-m/index.html" 2013(07/10) (2013).
[22] JOHNSON, P. and CHRISTY, R., "Optical Constants of Noble Metals" Phys.Rev.B 6(12), 4370-4379 (1972).
[23] Rheims, J., Koser, J. and Wriedt, T., "Refractive-index measurements in the near-IR using an Abbe refractometer" Meas Sci Technol 8(6), 601-605 (1997).
[24] Samoc, A., "Dispersion of refractive properties of solvents: Chloroform, toluene, benzene, and carbon disulfide in ultraviolet, visible, and near-infrared" J.Appl.Phys. 94(9), 6167-6174 (2003).
[25] Segelstein, D. J., "The complex refractive index of wate" University of Missouri-Kansas City (1981).
[26] Boreman, G. D., Johnson, T., Jones, A. C., Oh, S., Olmon, R. L., Raschke, M. B., Shelton, D. and Slovick, B., "Broadband Electrical Permittivity of Gold for Plasmonics and Nano-Optics Applications" Conference on Lasers and Electro-Optics (CLEO) (2011).
[27] Palik, E. D., [Handbook of Optical Constants of Solids], Academic Press, Boston (1997).
[28] Underwood, S. and Mulvaney, P., "Effect of the Solution Refractive-Index on the Color of Gold Colloids" Langmuir 10(10), 3427-3430 (1994).
[29] Kreibig, U., "Electronic Properties of Small Silver Particles - Optical-Constants and their Temperature-Dependence" Journal of Physics F-Metal Physics 4(7), 999-1014 (1974).
[30] Kelly, K. L., Coronado, E., Zhao, L. L. and Schatz, G. C., "The optical properties of metal nanoparticles: The influence of size, shape, and dielectric environment" J Phys Chem B 107(3), 668-677 (2003).
[31] Jain, P. K., Huang, X., El-Sayed, I. H. and El-Sayed, M. A., "Noble Metals on the Nanoscale: Optical and Photothermal Properties and Some Applications in Imaging, Sensing, Biology, and Medicine" Acc.Chem.Res. 41(12), 1578-1586 (2008).
[32] Link, S. and El-Sayed, M. A., "Shape and size dependence of radiative, non-radiative and photothermal properties of gold nanocrystals" International Reviews in Physical Chemistry 19(3), 409-453 (2000).
[33] McConnell, W. P., Novak, J. P., Brousseau, L. C., Fuierer, R. R., Tenent, R. C. and Feldheim, D. L., "Electronic and optical properties of chemically modified metal nanoparticles and molecularly bridged nanoparticle arrays" J Phys Chem B 104(38), 8925-8930 (2000).